RADIOMETRIC CROSS-CALIBRATION OF GAOFEN-1 WFV CAMERAS WITH LANDSAT-8 OLI AND MODIS SENSORS BASED ON RADIATION AND GEOMETRY MATCHING

Li Junping [1], Wu Zhaocong [2], Wei xin [1], Zhang Yi [2], Feng Fajie [1], Guo Feifei [2]

[1] Power China Hubei Electric Engineering Corporation, Wuhan, China
[2] School of Remote Sensing and Information Engineering, Wuhan University, Wuhan, China

KEY WORDS: Radiometric Cross-Calibration, Geometry Matching, Radiative Transfer Model, Water Vapor Effects, Synchronization Verification.

ABSTRACT:

Cross-calibration has the advantages of high precision, low resource requirements and simple implementation. It has been widely used in recent years. The four wide-field-of-view (WFV) cameras on-board Gaofen-1 satellite provide high spatial resolution and wide combined coverage (4×200km) without onboard calibration. In this paper, the four-band radiometric cross-calibration coefficients of WFV1 camera were obtained based on radiation and geometry matching taking Landsat 8 OLI (Operational Land Imager) sensor as reference. Scale Invariant Feature Transform (SIFT) feature detection method and distance and included angle weighting method were introduced to correct misregistration of WFV-OLI image pair. The radiative transfer model was used to eliminate difference between OLI sensor and WFV1 camera through the spectral match factor (SMF). The near-infrared band of WFV1 camera encompasses water vapor absorption bands, thus a Look Up Table (LUT) for SMF varies from water vapor amount is established to estimate the water vapor effects. The surface synchronization experiment was designed to verify the reliability of the cross-calibration coefficients, which seem to perform better than the official coefficients claimed by the China Centre for Resources Satellite Data and Application (CCRSDA).

1. INTRODUCTION

Now the acquisition of radiometric calibration coefficients for domestic satellites is still mostly dependent on vicarious calibration technique. However, vicarious calibration technique which involves quasi synchronous measurements is challenging because of its labour intensity, weather restriction, and high cost (Gong et al., 2011). Therefore, the calibration frequency is low, and it is basically maintained once a year, which restricts the quantitative application of all kinds of satellite products.

The radiometric cross calibration technique, taking a satellite sensor with high calibration precision as reference, is used to obtain radiometric calibration coefficients of the uncalibrated satellite sensor with low calibration precision (Gao et al., 2013). It has been widely used in recent years because of its high precision, low resource demand and simple manipulation. The reference satellite sensor and uncalibrated satellite sensor, involving in radiometric cross calibration, may vary in imaging geometry, spectral conditions, and atmospheric conditions. These differences can be eliminated by introducing the radiative transfer model which is called the RTM method.

The GF-1(GaoFen-1) satellite launched on April 26, 2013, with two panchromatic and multispectral (PMS) sensors and four wide-field-of-view (WFV) sensors on board, is the first satellite of Chinese high-resolution satellite constellation (Bai, 2014). The WFV cameras have irreplaceable advantages of relatively high spatial resolution (16m) and wide combined coverage (4×200km), which can be used in numerous applications. Due to the lack of onboard calibrators on the GF-1 satellite, the calibration coefficients for WFV cameras were published by The China Centre for Resources Satellite Data and Application (CRESDA) using vicarious calibration techniques. However, the lack of calibration precision and low calibration frequency limit the quantitative application of satellite products, which make the cross calibration a good choice for WFV cameras.

Based on the RTM method, the calibration coefficients of the Chinese Multi-channel Visible Infrared Scanning radiometer (MVIRS) sensor were obtained with viewing geometry correction using the bidirectional reflectance distribution function (BRDF) measured on the ground (Liu et al., 2014). A simple image-based method was proposed to calibrate WFV cameras with Landsat-8 OLI data as reference. To calculate the spectral match factor (SMF), the USGS spectral library was used to match the most appropriate hyperspectral data (Li et al., 2016). Considering the large view angles of WFV cameras (especially for WFV1 and WFV4), MODIS BRDF product was introduced to correct the unequal bidirectional effects. Extensive validations indicated that the uncertainty was within 8% for the cross-calibration coefficients (Feng et al., 2016).

In this paper, a cross-calibration method based on radiation and geometry matching was proposed to solve both the spectral matching problems caused by band coverage discrepancies and spectral response function (SRF) mismatches and the geometry matching problems caused by wide coverage of WFV1 camera. The four-band radiometric cross-calibration coefficients of WFV1 camera were obtained using the proposed method. While the surface synchronization experiment was designed to verify the reliability of the cross-calibration coefficients.

2. METHODOLOGY OF RADIOMETRIC CROSS CALIBRATION OF WFV1 CAMERA BASED ON RADIATION AND GEOMETRY MATCHING

2.1 Process of radiometric cross calibration of WFV1 camera based on radiation and geometry matching

The process of radiometric cross calibration of WFV1 camera based on radiation and geometry matching includes:

1. Sample points collecting. Get the radiance of OLI through the radiative calibration coefficients published in OLI image header file. For OLI-WFV1 image pair, the Scale Invariant

Feature Transform (SIFT) feature detection method is used to get feature points for OLI radiance image and WFV1 DN (Digital Number) image. Calculate the uniformity of image pixels respectively. For those points that pixel uniformity cumulative frequency lower 5%, select them as alternative points of sample points. Set weighted distance and mean value of included angles as the similarity measurement criteria to obtain sample points from alternative points.

2. SMF for sample points. For each sample point, get the spectral curve from the near-simultaneous hyperion data. Calculate the imaging geometry information and get the spectral response function both for OLI and WFV1 from public information. Download the MODIS Terra/Aqua Aerosol 5-Min L2 Swath 3km product from MODIS official website to get the aerosol optical depth (AOD) on the day of imaging. All of the above information is used as input for the 6S radiative transfer model to get SMFs that can eliminate the difference of OLI and WFV1 caused by imaging geometry, atmospheric conditions and spectral conditions. Then a Look Up Table (LUT) for SMFs vary from water vapor amount is established to estimate the water vapor effects. At last, water vapor amount on the imaging day obtained from MODIS 05 product is used to look for the corresponding SMF in the LUT and SMF for each sample point is obtained.
3. Radiative calibration coefficients fitting. Considering the linear design of the calibrated radiation characteristics of WFV1 camera, a linear fitting method is used to get the radiometric cross calibration coefficients.

The process is shown in Figure 1.

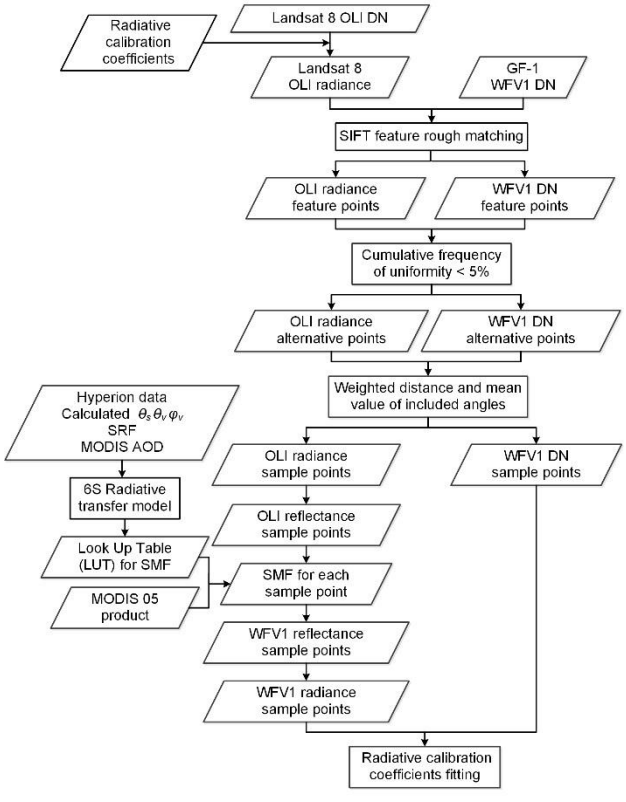

Figure 1. Process of radiometric cross calibration based on radiation and geometry matching

2.2 The selection of sample points

With feature points generated by using the Scale Invariant Feature Transform (SIFT) feature detection method, points with high uniformity are selected as alternative points of sample points. The uniformity for the specific pixel is defined as equation (1).

$$\varepsilon = \frac{S_{Std}}{S_{Mean}} \tag{1}$$

where ε = the uniformity for the specific pixel
S_{Std} = standard deviation of the eight surrounding pixels for the specific pixel
S_{Mean} = mean value of the eight surrounding pixels for the specific pixel

The L_{sim} composed of weighted distance and the mean value of included angles of the surrounding feature points is chosen as the similarity measurement criterion to obtain sample points from alternative points, as shown in equation (2).

$$L_{sim} = (D_W, \gamma_{mean}) \tag{2}$$

where L_{sim} = the similarity of the specific alternative point
D_W = weighted distance of the specific alternative point and surrounding feature points
γ_{Mean} = mean value of the included angles in radians

2.3 The calculation of SMF (Spectral Match Factor)

2.3.1 SMF: The SMF is defined as a ratio of TOA (top of atmosphere) reflectance, as shown in equation (3).

$$\alpha = \frac{\rho_{TOA_{aim}}}{\rho_{TOA_{ref}}} \tag{3}$$

where α= SMF (Spectral Match Factor)
$\rho_{TOA_{aim}}$ = TOA reflectance of uncalibrated satellite sensor, in this paper it refers to WFV1 camera
$\rho_{TOA_{ref}}$ = TOA reflectance of reference satellite sensor, in this paper it refers to Landsat 8 OLI

2.3.2 Inversion of TOA reflectance: The TOA reflectance of band i of the satellite sensor can be retrieved from the imaging geometry, the atmospheric parameters at imaging time and the spectral curve of the ground objects (Vermote et al., 2002), as shown in equation (4).

$$\rho_{TOA,i}(\theta_s,\theta_v,\phi_v) = T_{g,i}(\theta_s,\theta_v)\left(\rho_{R+A,i}(\theta_s,\theta_v,\phi_v) + \frac{\rho_{s,i}T_i(\theta_s)T_i(\theta_v)}{1-\rho_{s,i}S_i}\right) \tag{4}$$

where $\rho_{TOA,i}(\theta_s,\theta_v,\phi_v)$ = TOA reflectance of band i of the satellite sensor
θ_s,θ_v,ϕ_v = the solar zenith angle, the observation zenith angle and the relative azimuth angle between the sun and the satellite sensor at imaging time
$T_{g,i}(\theta_s,\theta_v)$ = transmissivity for atmospheric molecular absorption of band i of the satellite sensor
$\rho_{R+A,i}(\theta_s,\theta_v,\phi_v)$ = reflectance corresponding to atmospheric diffuse radiation of band i of the satellite sensor
$\rho_{s,i}$ = surface reflectance of the target of band i of the satellite sensor, it can be calculated with integral of spectral reflectance curve and SRF
$T_i(\theta_s)$ = total transmissivity of the descending radiation of band i of the satellite sensor

$T_i(\theta_v)$ = total transmissivity of the upgoing radiation of band i of the satellite sensor
S_i = the albedo of the atmosphere spherical surface of band i of the satellite sensor

Among these parameters, $\theta_s, \theta_v, \phi_v$ need to be calculated, $\rho_{s,i}$ can be obtained from hyperspectral data. The 6S radiative transfer model is used to get the remaining parameters through accurate parameters input.

2.3.3 Calculation of imaging geometry: The imaging geometry information referring in the header file is usually for the central pixel of image. Considering the wide range of WFV cameras, the difference of image geometry between the edge pixel and the central pixel is not negligible. In this paper, the solar zenith angle is calculated by the transit time of the satellite and the latitude and longitude of the corresponding pixel (Jacobson, 2005), as shown in equation (5).

$$\cos\theta_h = \sin(lat)\sin\delta + \cos(lat)\cos\delta\cos t \quad (5)$$

where θ_h= solar elevation angle, the complementary angle of the solar zenith angle θ_s, $\theta_s = \pi/2 - \theta_h$
lat = latitude of the corresponding pixel
δ = soar declination angle
t= solar hour angle at imaging time

The solar azimuth angle φ_s can be calculated through θ_h, δ and lat, as shown in equation (6).

$$\varphi_s = \arccos\left(\left[\sin\theta_h \sin(lat) - \sin\delta\right] / \cos\theta_h \cos(lat)\right) \quad (6)$$

The geometric angle of OLI and WFV1 camera at imaging time is shown in Figure 2. As the orbit height h and the range of observation zenith angle are known, the observation zenith angle of pixel to be solved (the corresponding red region in figure) can be calculated according to the distance between it and the edge pixel (the corresponding green region in figure).
For the GF-1 WFV1 camera, the observation zenith angle range is 24 ° to 40 ° (Feng et al., 2016). Considering the latitude and longitude information of WFV1 image pixel is not accurate, get the latitude and longitude by matching WFV1 image with the OLI image (without geometric correction).

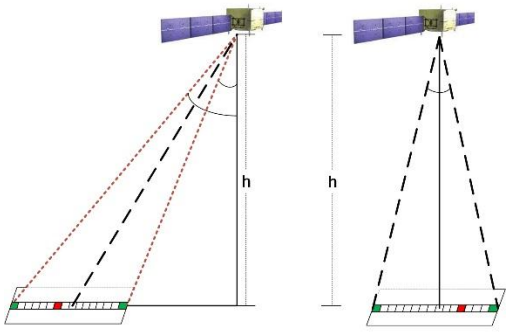

(a) (b)
Figure.2 The geometric angle of OLI and WFV1 camera at imaging time (a) WFV1 camera (b) Landsat 8 OLI

2.3.4 The Look Up Table (LUT) for SMF: The SMF is used to eliminate difference of OLI and WFV1 caused by imaging geometry, atmospheric conditions and spectral conditions. The imaging geometry has been discussed. The spectral conditions include spectral band coverage and spectral response function (SRF). The spectral response curves of the OLI sensor and WFV1 camera and a spectrum of total atmospheric transmission computed for midlatitude summer using 6S model are shown in Figure 3.
The OLI channels are spectrally narrower and their spectral positions are optimized to avoid atmospheric absorption features. This is especially true for the near-infrared band (ch4) where the WFV1 ch4 encompasses absorption bands of water vapor while the OLI ch4 is placed in a spectrally cleaner window.

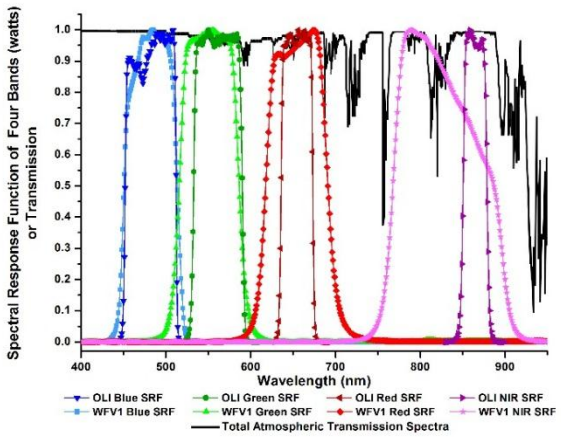

Figure.3 WFV1 and OLI spectral response functions with total atmospheric transmission spectra for midlatitude summer

The 6S radiative transfer model is run to estimate the water absorption effects. A midlatitude summer atmosphere is used and the water vapor amount is scaled by 0.01 to 5 times the nominal value to establish a Look Up Table (LUT) for SMF varies from water vapor amount.

2.4 Radiative calibration coefficients fitting

2.4.1 Calculation of TOA radiance: The TOA radiance of band i of WFV1 camera can be calculated from the TOA reflectance, as shown in equation (7).

$$L_{TOA,i} = \frac{E_{oi}\rho_{TOA,i}\cos\theta_s}{\pi ds^2} \quad (7)$$

where $L_{TOA,i}$ = TOA radiance of band i of WFV1 camera
$\rho_{TOA,i}$ = TOA reflectance of band i of WFV1 camera
E_{oi} = solar average spectral radiation at the top of the atmosphere for band i of WFV1 camera ($W \cdot m^{-2} \cdot \mu m^{-1}$)
ds = Earth-Sun Distance in astronomical units

ds can be calculated according to the ordinal date $days$ of the imaging date.

$$ds = 1 + 0.0167 \cdot \sin\left[2\pi \cdot (days - 93.5)/360\right] \quad (8)$$

2.4.2 Calibration coefficients fitting: The design of radiation characteristics of satellite sensors is generally linear, so as WFV1 camera. The radiometric calibration coefficients of band i can be fitted according to the above mentioned calculated TOA radiance and corresponding DN of WFV1 camera, as shown in equation (9).

$$L_{TOA,i} = Gain_i * DN_i + Offset_i \quad (9)$$

where $Gain_i, Offset_i$ = radiometric calibration coefficients of band i of WFV1 camera

3. RADIOMETRIC CROSS CALIBRATION OF GF-1 WFV1 CAMERA

3.1 Data

The experimental area used for cross radiation calibration must be flat and uniform, with the type of ground objects single. The Dunhuang calibration site (40.07 ° N, 94.32 ° E), located in the Gobi Desert in northwest China, is one of the calibration sites commonly used. The calibration site is situated on an alluvial fan, basically composed of gravel and sparse vegetation edge-covered (He et al., 1997). The uniformity of the site has been verified through the coefficient of variation (<2%) and the measured reflectance data of the satellite images (Hu et al., 2010). Considering the uniformity of the Dunhuang calibration site, it was chosen as the experimental area in this paper. Some research has found that the calibration site is a continental climate, basically corresponding to the desert aerosol model and contains a slight continental aerosol (Hu et al., 2001; Min et al., 2002).
The OLI-WFV1 image pair, covering the Dunhuang calibration site on the same imaging day, is selected to carry out radiometric cross calibration experiments. The image information is shown in Table 1.

Image Information	GF-1 WFV	Landsat8 OLI
Imaging time(GMT)	2014-10-15 04:43:22	2014-10-15 04:26:27
Row and column	13400 * 12000	7861 * 7721
Geographic coordinate system and projection	WGS-84 RFM	WGS-84 UTM 46 N

Table 1. Image information

The location of the calibration site on the OLI image and WFV1 image is shown in Figure 4.

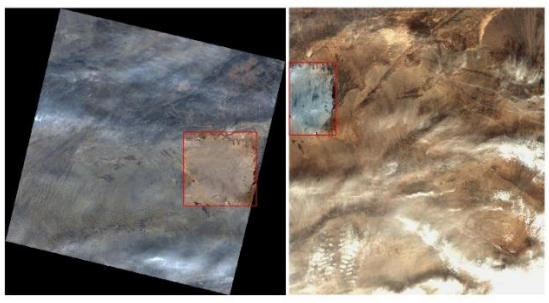

(a) (b)
Figure.4 The location of the calibration site
(a) Landsat 8 OLI (b) GF-1 WFV1

3.2 Sample points

For OLI-WFV1 image pair, 135 pairs of feature point were generated by using the Scale Invariant Feature Transform (SIFT) feature detection method.
Calculate the uniformity of image pixels respectively for OLI radiance image and WFV1 DN image. Points with cumulative frequency of uniformity lower 5% were selected as alternative points of sample points, as shown in Figure 5. The uniformity thresholds according to 5% are respectively 0.23 and 2.79 for OLI image and WFV1 image, with 194260 alternative points for OLI image and 387795 alternative points for WFV1 image.
500 pairs of sample points were selected using method mentioned in equation (2).

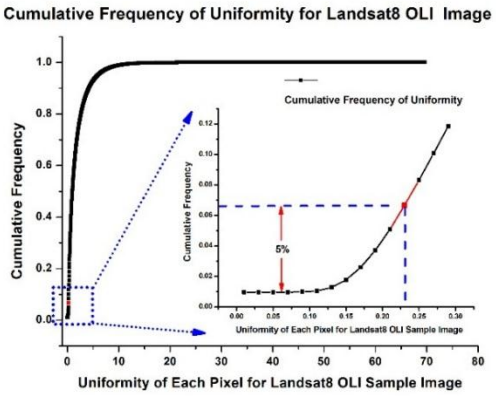

(a)

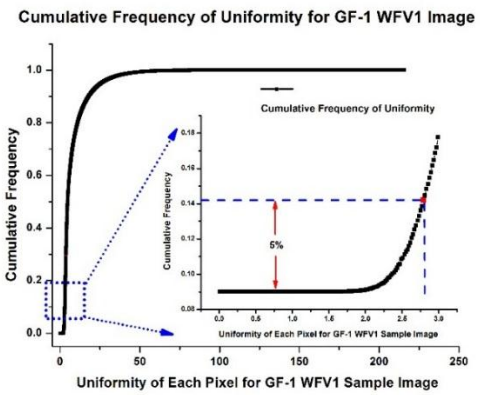

(b)
Figure.5 Cumulative frequency of uniformity
(a) Landsat 8 OLI (b) GF-1 WFV1

3.3 TOA radiance for sample points

Suppose the atmospheric conditions were not changed during the imaging time interval (17min) between the Landsat 8 OLI and GF-1 WFV1. The imaging geometry was calculated as mentioned in 2.3.3 section. The spectral response functions (SRFs) of OLI sensor and WFV1 camera were obtained from the USGS website and the China Resource Satellite Center website respectively. The elevation information of sample points from ASTER GDEM data was also used as an input of 6S model. The AOD data from MODIS Terra/Aqua Aerosol 5-Min L2 Swath 3km product and water vapor amount from MODIS 05 product were input as atmospheric parameters.
The TOA reflectance of sample points was obtained as mentioned in 2.3.2 section. The E_{oi} ($W \cdot m^{-2} \cdot \mu m^{-1}$) of WFV1 camera used for calculating TOA radiance was shown in Table 2.

	Blue	Green	Red	NIR
E_{oi}	1968.66	1849.43	1570.88	1078.97

Table 2. E_{oi} for WFV1 camera

3.4 Cross calibration coefficients fitting

The radiometric cross calibration coefficients of WFV1 camera were fitted as shown in Figure 6.

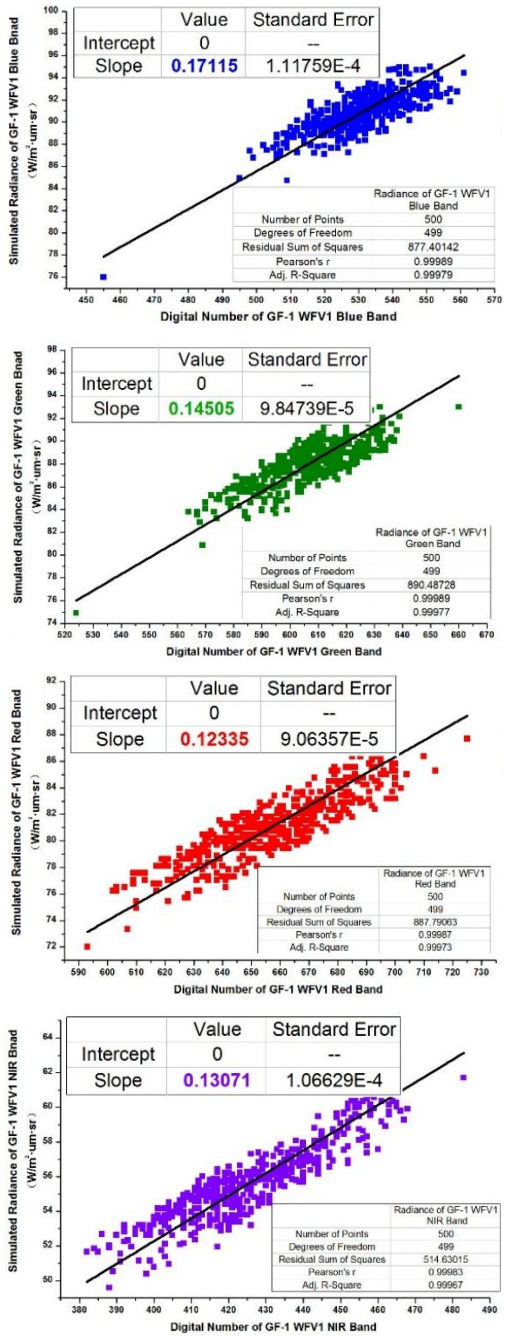

Figure.6 The fitted radiometric cross calibration coefficients of WFV1 camera

The crosscalibration coefficients were also compared with the calibration coefficients published by the China Centre for Resources Satellite Data and Application (CCRSDA), as shown in Table 3.

calibration coefficients	Blue	Green	Red	NIR
CCRSDA	0.2004	0.1648	0.1243	0.1563
This paper	0.17115	0.14505	0.12335	0.13071

Table 3. Calibration coefficients for CCRSDA and this paper

3.5 Validation of cross calibration coefficients

The GF-1 WFV1 image covering Songshan area on October 24, 2014 is selected to conduct validation experiment of cross calibration coefficients. The imaging date is close to the radiometric cross calibration imaging date, which makes it more reliable.

The spectral reflectance of 36 sample areas were collected using ASD Field Spec 4 spectrometer from October 10 to October 31, in the Songshan area of Dengfeng City, Henan Province. A clear and cloudless weather was selected and five spectral data were measured at each sample point with a sample point interval of 3m. Four rounds of spectral measurements were carried out in each sample area, and total 91865 spectra were measured at last. The atmospheric optical data was also measured from 8:30 to 17:00 everyday by using the CE318 sun photometer.

The 36 sample areas contain 14 kinds of objects. Some examples are shown in Figure 7.

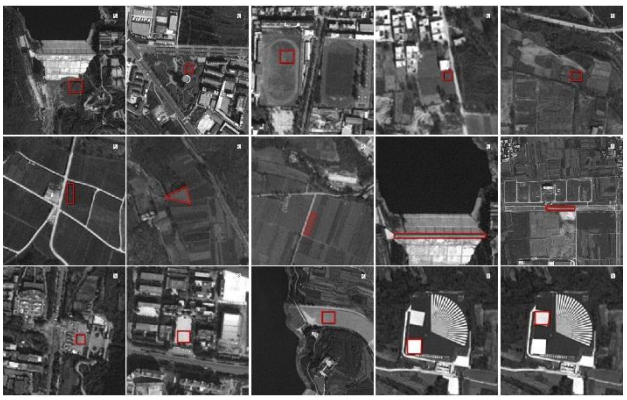

Figure.7 Examples of 14 kinds of objects (the last two pictures refering to the two targets of Songshan calibration field, are the same object)

The spectral reflectance measured by the spectrometer is a continuous curve, while the reflectance obtained from satellite image after radiometric correction marked as ρ_c is discrete. To make a better comparison between the continuous spectral curve and discrete reflectance ρ_c, a convolution of the SRF for the specific band of the WFV1 camera and the measured continuous spectral curve was conducted to get a discrete reflectance marked as ρ_t, which was regarded as the ground truth value. If the spectral measurements had been collected on October 24, the convolutional ρ_t can be compared with ρ_c directly. Otherwise, the inverse-distance weighted mean value of the two ρ_t for two days that close to October 24 was regarded as ρ_t of October 24. The aerosol optical depth (AOD) was retrieved by the Langley method, while the AOD at 550nm was interpolated from AOD at other wavelengths.

The reflectance ρ_c obtained after atmospheric correction based on the radiometric cross calibration coefficients in this paper was compared with ρ_t to get the relative difference between ρ_c and ρ_t, which was marked as R_d. For further comparison, the R_d for calibration coefficients published by the CCRSDA was also calculated. The mean R_d of 36 sample areas for four bands of WFV1 camera were shown in Table 4.

R_d	Blue	Green	Red	NIR
CCRSDA	65.52%	29.78%	32.43%	19.57%
This paper	39.21%	24.82%	32.06%	19.35%

Table 4. The mean R_d for 36 sample areas

The mean R_d for 36 sample areas corresponding to cross calibration coefficients is lower than calibration coefficients published by the CCRSDA, especially for the blue band, which is reasonable as the band with shorter wavelength will be more affected by the atmosphere.

The ρ_c obtained from cross calibration coefficients (the corresponding red point in figure), along with ρ_c obtained from calibration coefficients published by the CCRSDA (the corresponding green triangle in figure), were compared with the continuous reflectance curve measured by the spectrometer, as shown in Figure 8. It is obvious that the cross calibration coefficients perform better than the calibration coefficients claimed by the CCRSDA.

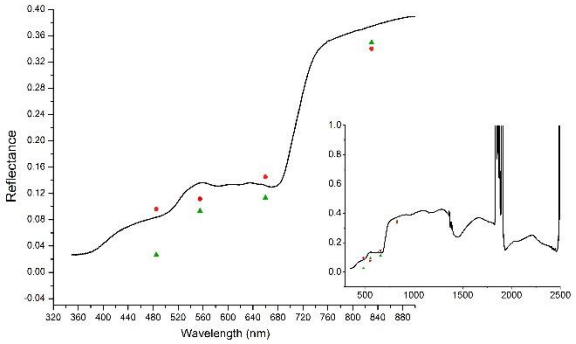

Figure.8 The comparision of ρ_c for a specific sample area

4. DISSCUSSION

In the 3.5 section, we compared the cross calibration coefficients obtained in this paper with the calibration coefficients claimed by the CCRSDA. Both statistical results and graphic display have indicated that the former may perform better in the quantitative applications. For the blue band, the mean value of R_d for calibration coefficients of the CCRSDA can reach a large amount of 65.52%, which is quite different from the ground truth. To explore the causes of this problem, calibration coefficients of other three years (2013, 2015 and 2016) claimed by the CCRSDA were also compared with the cross calibration coefficients obtained in this paper, as shown in Table 5. It is obvious that the cross calibration coefficients (in bold) obtained in this paper is more consistent with the changing trend of the calibration coefficients for the other three years, which may be the reason for the large deviation of the calibration coefficients for 2014.

calibration coefficients	Blue	Green	Red	NIR
2013	0.1709	0.1398	0.1195	0.1338
2014	0.2004	0.1648	0.1243	0.1563
2015	0.1816	0.156	0.1412	0.1368
2016	0.1843	0.1477	0.122	0.1365
This paper	**0.17115**	**0.14505**	**0.12335**	**0.13071**

Table 5. The comparision of calibration coefficients

5. CONCLUSIONS

A radiometric cross calibration method based on radiation and geometry matching has been proposed to get the calibration coefficients of GF-1 WFV1 camera taking Landsat 8 OLI sensor as reference. With the surface synchronization experiment data, it is proved that the cross calibration coefficients perform better than calibration coefficients claimed by the CCRSDA, which also confirms the validity of the radiometric cross calibration method. Cosidering the unique imaging geometry of GF-1 WFV1 camera, the method can also be used for other domestic remote sensing satellites.

REFERENCES

Bai Zhaoguang, J., 2014. The design and characteristics of Gaofen-1 satellite. *Space International*, (3), pp.12-19.

Feng L, Li J, Gong W, et al., J., 2016. Radiometric cross-calibration of Gaofen-1 WFV cameras using Landsat-8 OLI images: A solution for large view angle associated problems. *Remote Sensing of Environment*, 174, pp. 56-68.

Gao Caixia, Jiang Xiaoguang, Ma Lingling, et al., J., 2013. Review of radiometric cross-calibration. *Arid Land Geography*, 36(1), pp. 139-146.

Gong Hui, Tian Guoliang, Yu Tao, et al., J., 2011. Radiometric Calibration and Validation of CCD Cameras on HJ-1 Satellite. *Remote Sensing Technology and Application*, 26(5), pp. 682-688.

He Jitai, Lu Yihuai, J., 1997. The Measurement and Evaluation of Bidirectional Reflectance Characteristics of Dunhuang Radiative Calibration Site. *Journal of Remote Sensing*, 1(4), pp. 246-251.

Hu X, Liu J, Sun L, et al., J., 2010. Characterization of CRCS Dunhuang test site and vicarious calibration utilization for Fengyun (FY) series sensors. *Canadian Journal of Remote Sensing*, 36(5), pp. 566-582.

Hu Xiuqing, Zhang Yuxiang, Zhang Guangshun, et al., J., 2001. Measurements and Study of Aerosol Optical Characteristics in China Radiometric Calibration Sites. *Quarterly Journal of Applied Meteorology*, 12(3), pp. 257-266.

Jacobson M Z, M., 2005. Fundamentals of atmospheric modelling. *Cambridge: Cambridge University Press*, pp. 317.

Li J, Feng L, Pang X, et al., J., 2016. Radiometric cross Calibration of Gaofen-1 WFV Cameras Using Landsat-8 OLI Images: A Simple Image-Based Method. *Remote Sensing*, 8(5), pp. 411.

Liu J J, Li Z, Qiao Y L, et al., J., 2004. A new method for cross-calibration of two satellite sensors. *International Journal of Remote Sensing*, 25(23), pp. 5267-5281.

Min Xiangjun, Wang Zhimin, Fu Qiaoyan, et al., J., 2002. Ground Simultaneous Measurements and Analysis of Radiometric Characterization of Dunhuang Test Site for Calibrating CBERS-1 Sensors. *Geo-Information Science*, 4(3), pp. 43-50.

Vermote E F, Tanre D, Deuze J L, et al., J., 2002. Second Simulation of the Satellite Signal in the Solar Spectrum, 6S: an overview. *IEEE Transactions on Geoscience & Remote Sensing*, 35(3), pp. 675-686.